Synchronous X-ray and Radio Mode Switches: A Rapid Global Transformation of the Pulsar Magnetosphere

W. Hermsen *et al.*

Science **339**, 436 (2013);
DOI: 10.1126/science.1230960

Synchronous X-ray and Radio Mode Switches: A Rapid Global Transformation of the Pulsar Magnetosphere

W. Hermsen,[1,2]* J. W. T. Hessels,[2,3] L. Kuiper,[1] J. van Leeuwen,[2,3] D. Mitra,[4] J. de Plaa,[1] J. M. Rankin,[2,5] B. W. Stappers,[6] G. A. E. Wright,[7] R. Basu,[4] A. Alexov,[8] T. Coenen,[2] J.-M. Grießmeier,[9,10] T. E. Hassall,[6,11] A. Karastergiou,[12] E. Keane,[13] V. I. Kondratiev,[3,14] M. Kramer,[6,13] M. Kuniyoshi,[13] A. Noutsos,[13] M. Serylak,[9,10] M. Pilia,[3] C. Sobey,[13] P. Weltevrede,[6] K. Zagkouris,[12] A. Asgekar,[3] I. M. Avruch,[1,3,15] F. Batejat,[16] M. E. Bell,[11,17] M. R. Bell,[18] M. J. Bentum,[3,19] G. Bernardi,[20] P. Best,[21] L. Bîrzan,[22] A. Bonafede,[23] F. Breitling,[24] J. Broderick,[11] M. Brüggen,[23] H. R. Butcher,[3,25] B. Ciardi,[18] S. Duscha,[3] J. Eislöffel,[26] H. Falcke,[3,13,27] R. Fender,[11] C. Ferrari,[28] W. Frieswijk,[3] M. A. Garrett,[3,22] F. de Gasperin,[23] E. de Geus,[3] A. W. Gunst,[3] G. Heald,[3] M. Hoeft,[26] A. Horneffer,[13] M. Iacobelli,[22] G. Kuper,[3] P. Maat,[3] G. Macario,[28] S. Markoff,[2] J. P. McKean,[3] M. Mevius,[3,15] J. C. A. Miller-Jones,[2,29] R. Morganti,[3,15] H. Munk,[3] E. Orrú,[3,27] H. Paas,[30] M. Pandey-Pommier,[22,31] V. N. Pandey,[32] R. Pizzo,[3] A. G. Polatidis,[3] S. Rawlings,[12] W. Reich,[13] H. Röttgering,[22] A. M. M. Scaife,[11] A. Schoenmakers,[3] A. Shulevski,[15] J. Sluman,[3] M. Steinmetz,[24] M. Tagger,[9] Y. Tang,[3] C. Tasse,[33,34,35] S. ter Veen,[27] R. Vermeulen,[3] R. H. van de Brink,[3] R. J. van Weeren,[3,20,22] R. A. M. J. Wijers,[2] M. W. Wise,[2,3] O. Wucknitz,[13,36] S. Yatawatta,[3] P. Zarka[33]

Pulsars emit from low-frequency radio waves up to high-energy gamma-rays, generated anywhere from the stellar surface out to the edge of the magnetosphere. Detecting correlated mode changes across the electromagnetic spectrum is therefore key to understanding the physical relationship among the emission sites. Through simultaneous observations, we detected synchronous switching in the radio and x-ray emission properties of PSR B0943+10. When the pulsar is in a sustained radio-"bright" mode, the x-rays show only an unpulsed, nonthermal component. Conversely, when the pulsar is in a radio-"quiet" mode, the x-ray luminosity more than doubles and a 100% pulsed thermal component is observed along with the nonthermal component. This indicates rapid, global changes to the conditions in the magnetosphere, which challenge all proposed pulsar emission theories.

Radio pulsars are powered by the energy released as the highly magnetized neutron star spins down. The radio pulses are generated in the pulsar magnetosphere, probably close to the neutron star surface (*1*, *2*). Shortly after the discovery of pulsars, it was observed that the radio pulse behavior can discretely change on time scales as short as a rotation period. These changes in emission mode can manifest as switches between ordered and disordered states or variations in intensity and pulse shape, including the complete cessation of observable radio emission (*3*, *4*).

Because the emitted radio luminosity is a negligible fraction of the available spin-down energy, usually substantially less than 10^{-5}, this phenomenology was presumed to be related solely to microphysics of the radio emission mechanism itself. This perception has recently been challenged by the identification of a relationship between the spin properties of neutron stars and their radio emission modes. PSR B1931+24 was observed to cease emitting for tens of days, during which it spins down ~50% less rapidly (*5*). PSR J1841–0500 (*6*) and PSR J1832+0029 (*7*) exhibit similar behaviors. A number of other pulsars display smaller changes in spin-down rate, which correlate with variations in their average radio pulse shapes (*8*). The implication of these results is that mode changing is due to an inherent, perhaps universal pulsar process that causes a sudden change in the rate of angular momentum loss, which is communicated along the open field lines of the magnetosphere. Whereas changes in spin-down rate can only be detected on time scales of a few days or longer, the recently identified link with the rapid switching observed in radio emission modes suggests a transformation of the global magnetospheric state in less than a rotation period. Despite the recent flurry of pulsar detections at high energies (*9*), the only causal relation between the radio pulses and emission at other wavelengths, likely emanating from different locations in the magnetosphere, has been made for optical emission and giant radio pulses from the Crab pulsar (*10*).

PSR B0943+10 is a paragon of mode-changing pulsars. Relatively old (characteristic age 5 million years), with a long spin period (1.1 s), it switches at intervals of several hours between a radio-bright, highly organized mode (B) and a quieter chaotic mode (Q) (*11*, *12*). At the B- to Q-mode transition, a subpulse drifting structure dissolves within a few seconds, the emission becomes disorganized, and an additional highly polarized radio component appears, preceding the main pulse by 52° of pulse longitude (*13*). PSR B0943+10 has also been detected in two short observations with the XMM-Newton observatory as a weak x-ray source (*14*). These observations, under the assumption that the x-rays are thermal, were used to support a model in which one system of streaming particles produces the subpulse-modulated radio emission directly, and also results in thermal x-ray emission through bombardment of the polar cap surface (*15*). Because the particle streams are thought to be determined by the magnetosphere as a whole, detection of simultaneous x-ray and radio mode switching would uniquely probe the interaction between local and global electromagnetic behavior. Moreover, this would

[1]SRON, Netherlands Institute for Space Research, Sorbonnelaan 2, 3584 CA Utrecht, Netherlands. [2]Astronomical Institute "Anton Pannekoek," University of Amsterdam, Postbus 94249, 1090 GE Amsterdam, Netherlands. [3]ASTRON, Netherlands Institute for Radio Astronomy, Postbus 2, 7990 AA Dwingeloo, Netherlands. [4]National Centre for Radio Astrophysics (NCFRA-TIFR), Post Bag 3, Ganeshkhind, Pune University Campus, Pune 411007, India. [5]Physics Department, University of Vermont, Burlington, VT 05405, USA. [6]Jodrell Bank Center for Astrophysics, School of Physics and Astronomy, University of Manchester, Manchester M13 9PL, UK. [7]Astronomy Centre, University of Sussex, Falmer, Brighton BN1 9QJ, UK. [8]Space Telescope Science Institute (STScI), 3700 San Martin Drive, Baltimore, MD 21218, USA. [9]Laboratoire de Physique et Chimie de l'Environnement et de l'Espace, LPC2E CNRS/Université d'Orléans, 45071 Orléans Cedex 02, France. [10]Station de Radioastronomie de Nançay, Observatoire de Paris, CNRS/INSU, 18330 Nançay, France. [11]School of Physics and Astronomy, University of Southampton, Southampton SO17 1BJ, UK. [12]Astrophysics, University of Oxford, Oxford OX1 3RH, UK. [13]Max-Planck-Institut für Radioastronomie, Auf dem Hügel 69, 53121 Bonn, Germany. [14]Astro Space Center of the Lebedev Physical Institute, Profsoyuznaya str. 84/32, Moscow 117997, Russia. [15]Kapteyn Astronomical Institute, P.O. Box 800, 9700 AV Groningen, Netherlands. [16]Onsala Space Observatory, Department of Earth and Space Sciences, Chalmers University of Technology, SE-43992 Onsala, Sweden. [17]ARC Centre of Excellence for All-Sky Astrophysics (CAASTRO), Sydney Institute of Astronomy, University of Sydney, Sydney, NSW 2006, Australia. [18]Max Planck Institute for Astrophysics, Karl Schwarzschild Str. 1, 85741 Garching, Germany. [19]University of Twente, P.O. Box 217, 7500 AE Enschede, Netherlands. [20]Harvard-Smithsonian Center for Astrophysics, 60 Garden Street, Cambridge, MA 02138, USA. [21]Institute of Astronomy, University of Edinburgh, Royal Observatory of Edinburgh, Blackford Hill, Edinburgh EH9 3HJ, UK. [22]Leiden Observatory, Leiden University, P.O. Box 9513, 2300 RA Leiden, Netherlands. [23]Hamburger Sternwarte, University of Hamburg, Gojenbergsweg 112, 21029 Hamburg, Germany. [24]Leibniz-Institut für Astrophysik Potsdam (AIP), An der Sternwarte 16, 14482 Potsdam, Germany. [25]Research School of Astronomy and Astrophysics, Australian National University, Mt. Stromlo Observatory, via Cotter Road, Weston, ACT 2611, Australia. [26]Thüringer Landessternwarte, Sternwarte 5, D-07778 Tautenburg, Germany. [27]Department of Astrophysics/IMAPP, Radboud University Nijmegen, P.O. Box 9010, 6500 GL Nijmegen, Netherlands. [28]Laboratoire Lagrange, UMR7293, Université de Nice Sophia-Antipolis, CNRS, Observatoire de la Côte d'Azur, 06300 Nice, France. [29]International Centre for Radio Astronomy Research, Curtin University, G.P.O. Box U1987, Perth, WA 6845, Australia. [30]Center for Information Technology (CIT), University of Groningen, 9747 AJ Groningen, Netherlands. [31]Centre de Recherche Astrophysique de Lyon, Observatoire de Lyon, 9 av. Charles André, 69561 Saint Genis Laval Cedex, France. [32]National Radio Astronomy Observatory, 520 Edgemont Road, Charlottesville, VA 22903, USA. [33]LESIA-Observatoire de Paris, CNRS, UPMC Université Paris-Diderot, 92190 Meudon, France. [34]Department of Physics and Electronics, Rhodes University, P.O. Box 94, Grahamstown 6140, South Africa. [35]SKA South Africa, 3rd Floor, The Park, Park Road, Pinelands 7405, South Africa. [36]Argelander-Institut für Astronomie, University of Bonn, Auf dem Hügel 71, 53121 Bonn, Germany.

*To whom correspondence should be addressed. E-mail: w.hermsen@sron.nl

strengthen the earlier conclusion that entire magnetospheres change, settling down within a few seconds.

To test these hypotheses, we carried out a simultaneous x-ray and radio observing campaign on PSR B0943+10 from 4 November to 4 December 2011. These observations were designed to investigate what changes, if any, occurred in the x-rays when the radio emission changed mode. The x-ray observations consisted of six 6-hour observations in the 0.2- to 10-keV energy band with ESA's XMM-Newton space observatory (*16*) (table S1), accompanied by radio observations with the Giant Metrewave Radio Telescope (GMRT) in India at 320 MHz and the international Low Frequency Array (LOFAR) at 140 MHz, both simultaneously.

To identify the radio B- and Q-mode time windows, we folded the radio pulse sequences with up-to-date ephemerides from the Jodrell Bank long-term timing program (*17*) (Fig. 1). We could determine the times of mode switches from GMRT and LOFAR data with an accuracy of a few seconds. Table S2 lists the used B- and Q-mode time windows, which completely cover our XMM-Newton observations. In the ~30 hours of usable x-ray observations, PSR B0943+10 spent roughly equal amounts of time in the B and Q modes.

PSR B0943+10 was clearly detected in each of our XMM-Newton observations with the simultaneously used charge-coupled device (CCD) detectors PN (*18*) and MOS-1+2 (*19*) of the European Photon Imaging Camera (EPIC). The derived count rates ranged from that of the previously reported value for the PN detector of 0.38 (±0.07) × 10^{-2} counts/s (0.5 to 8 keV) (*14*) up to about twice that value, providing evidence for x-ray variability in an old, rotation-powered pulsar. Dividing the 0.2- to 10-keV x-ray events into the radio-derived B- and Q-mode time windows, we found the x-ray count rate to be higher in the radio Q mode than in the B mode by more than a factor of 2 (fig. S1). In the B mode, the PN CCDs had a count rate of 0.44 (±0.07) × 10^{-2} counts/s, whereas in the Q mode this more than doubled to 1.08 (±0.08) × 10^{-2} counts/s. This finding was independently confirmed with the MOS detectors, providing evidence for simultaneous mode switching in the radio and x-ray properties.

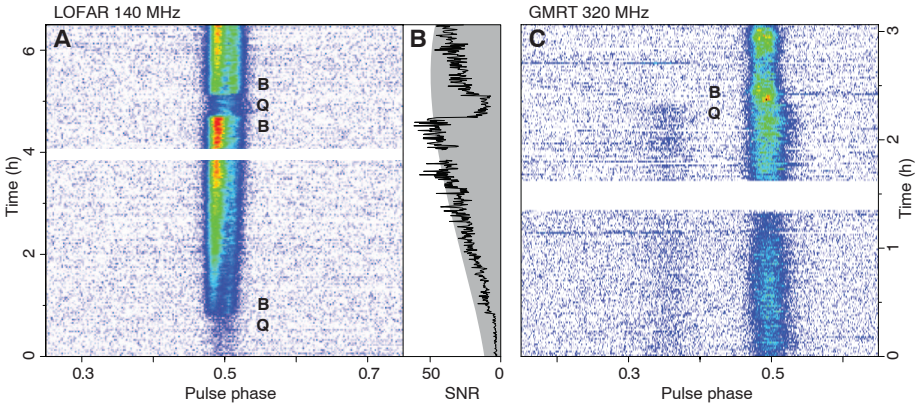

Fig. 1. (**A**) Identification of the B and Q modes with LOFAR at 140 MHz during XMM-Newton observation 1, showing pulse intensity versus rotational phase and time. A 10-min section (at the 4-hour mark) contaminated by interference is blanked out. (**B**) Comparison of the measured signal-to-noise ratio (SNR) and the nominal relative LOFAR sensitivity, changing with elevation throughout the observation (gray scale), normalized over the 4.0- to 4.5-hour range. (**C**) GMRT detection at 320 MHz of a Q- to B-mode transition in XMM-Newton observation 5. Color scale is optimized to show the simultaneous disappearance of the precursor pulse at phase ~0.35. A 15-min section (at the 1.5-hour mark) used for rephasing on a continuum source is blanked out.

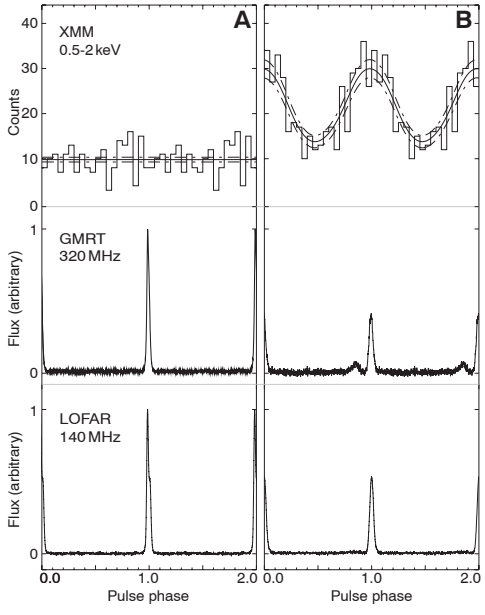

Fig. 2. Aligned x-ray and radio pulse profiles of PSR B0943+10 in its B and Q modes. (**A**) B mode: There is no evidence for a pulsed signal in the B-mode x-ray data, the flat distribution showing constant emission from the pulsar. (**B**) Q mode: The x-ray profile in the Q mode represents a 6.6σ detection on top of a flat constant level. The solid and dashed lines in the x-ray profiles are the kernel density estimator and ±1σ levels. The weak precursor, present only in the Q mode, is clearly visible in the GMRT radio profile at 320 MHz at 52° (0.14 phase) prior to the main pulse, and verified to be also weakly present in the LOFAR Q-mode profile.

To search for x-ray pulsations, we selected events recorded by the PN and MOS-1+2 CCDs that arrived in the Q-mode time window and within a radius of 15 arc sec from the source position. From this, we obtained a 6.6σ detection of a pulsed signal (Fig. 2B, top) at a period consistent with the rotational frequency predicted by the Jodrell Bank ephemeris (table S3). The pulse profile (energies of 0.5 to 2 keV) is broad. Surprisingly, the x-ray events detected during the radio B mode do not show any evidence for a pulsed signal (Fig. 2A, top). Figure 2 shows that the broad x-ray pulse in the Q mode covers the phases of the main radio pulse and precursor; the latter is clearly visible in the Q mode, 52° (0.14 phase) ahead of the main pulse at 320 MHz (Fig. 2B).

X-ray spectral analysis (*16*) revealed two components in the Q mode. The best spectral fit to the total (i.e., pulsed and unpulsed) spectrum is the sum of a power-law component and a thermal blackbody component (Fig. 3A; fit parameters in Table 1 and table S4). The spectrum of the pulsed component in the Q mode is best described by a single thermal blackbody model (Fig. 3B, Table 1, and table S4). It appears that the spectral fits to the thermal component in the total Q-mode spectrum and the thermal pulsed spectrum in the Q mode are statistically consistent (Δ flux = 0.1σ, $\Delta kT = 2.5\sigma$). This means that the Q-mode total x-ray emission consists of an unpulsed component with a steep, nonthermal power-law spectrum, and a ~100% pulsed component with a thermal blackbody spectrum. This is also reflected in the variation of the pulsed fraction with energy (table S5). In the B mode, the spectrum can be satisfactorily described with a single power law as well as a single blackbody shape (table S4). However, the most likely shape is a nonthermal spectrum (Fig. 3C), indistinguishable from the nonthermal component in the total Q-mode spectrum (supplementary text).

PSR B0943+10 is one of only 10 old (characteristic age >1 million years), nonrecycled radio pulsars where x-ray emission has also been detected (*20*–*22*). Although the surfaces of such pulsars have cooled substantially since birth, the observed x-ray emission is argued to be thermal in

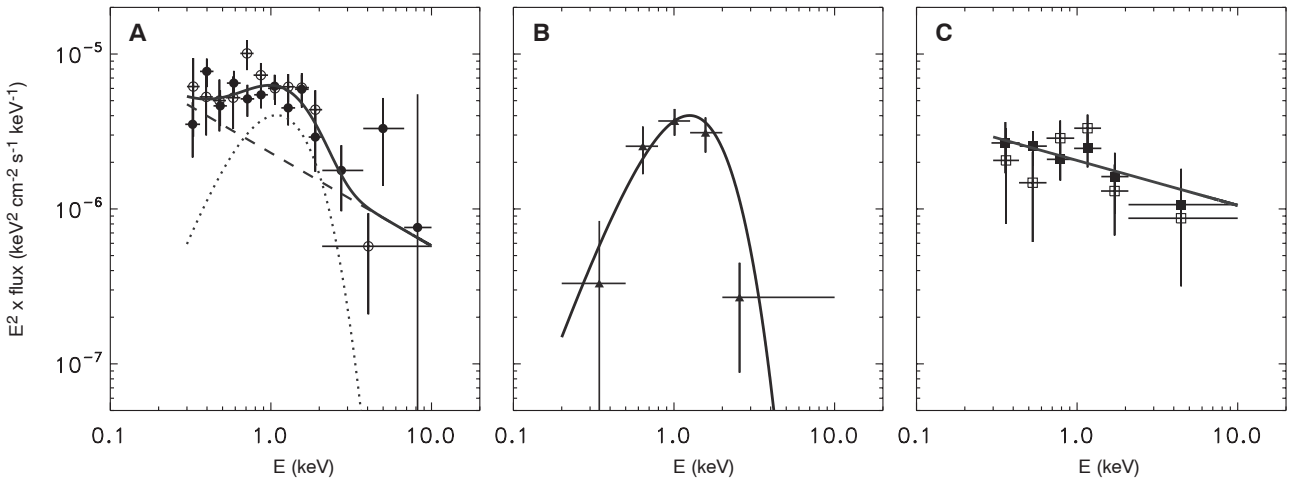

Fig. 3. Unabsorbed (i.e., corrected for absorption by interstellar gas along the line of sight) x-ray photon spectra of PSR B0943+10. (**A**) Total (i.e., pulsed and unpulsed) spectrum from spatial analyses of skymaps of Q-mode events from the XMM EPIC PN CCDs (solid symbols) and MOS1+2 CCDs (open symbols). The solid line shows the best model fit consisting of a power-law component (broken line) and a blackbody component (dotted line). (**B**) The spectrum of the pulsed emission detected only in the Q mode, analyzing the pulse profiles measured with the PN and MOS1+2 CCDs. The solid curve shows the best blackbody fit. (**C**) The total spectrum, as in (A), but here for the B-mode time windows. The solid line shows the best-fit power-law spectrum. The thermal blackbody components in (A) and (B) are statistically the same; the nonthermal power-law components in (A) and (C) are also fully consistent with being identical. All error bars are 1σ. For fit parameters, see Table 1.

Table 1. Spectral parameters for the best model fits to the x-ray spectra shown in Fig. 3. Fits are made with a blackbody (BB) shape and/or a power-law (PL) shape for the total and the pulsed emissions in the Q-mode window and the total emission in the B-mode. The column density N_H has been fixed at 4.3×10^{20} cm^{-2}. Flux values are given for energies 0.5 to 8 keV.

Mode	Model	BB (kT) (keV)	PL index Γ ($\alpha E^{-\Gamma}$)	BB flux, unabs. (10^{-15} erg cm^{-2} s^{-1})	PL flux, unabs. (10^{-15} erg cm^{-2} s^{-1})	χ^2_{red} (df)
Q total	BB + PL	0.277 ± 0.012	2.60 ± 0.34	7.52 ± 2.20	7.55 ± 1.81	0.81 (20)
Q pulsed	BB	0.319 ± 0.012	—	7.81 ± 1.64	—	0.38 (3)
B total	PL	—	2.29 ± 0.16	—	7.69 ± 1.00	0.74 (10)

some cases. This has led to the conclusion that such pulsars may have "hotspots" on their magnetic polar caps, generated by the bombardment of particles accelerated in the radio emission process. In all models, the bombarding particles result from pair creation in the pulsar magnetosphere. In polar vacuum gap models (*1*, *23*), this occurs directly above the surface. Recent adaptations of the model (*15*) predict the thermal x-ray brightness of pulsars that exhibit regular modulation of their radio subpulse drift. Such modulation is indeed observed in the B mode of PSR B0943+10 (*24*), and the original x-ray detection of this pulsar (*14*) was considered to support this prediction under the assumption that the x-rays have a thermal origin. However, the reported count rate suggests that the pulsar was in the B mode during those observations, whereas our spectral analysis shows that the x-ray emission in the B mode is actually nonthermal. Surprisingly, we detect strong thermal x-rays only in the Q mode, where the observed radio emission is weak and chaotic.

Space charge–limited flow models (*2*) also feature pair-created particles that heat the polar cap via backflow. These differ from polar gap models, however, in that charged primary particles are freely drawn from the neutron star surface. The thermal luminosities predicted for older pulsars (*25*) fall below what is observed in PSR B0943+10's Q mode and below the model's expected nonthermal cascade emission, consisting of contributions from curvature radiation, inverse Compton scattering, and synchrotron radiation (*26*). Such nonthermal emission, expected on open field lines, would almost certainly be mode-dependent, in contrast to what we observe.

Modeling of PSR B0943+10's geometry (*27*) strongly argues that the magnetic and spin axes are nearly aligned, with our line of sight passing near the pole (*24*) (Fig. 4A). This implies that the isotropically emitted x-rays of a polar hotspot should appear unmodulated throughout the rotation period, contrary to the observed Q-mode x-ray pulsations. One possible implication is that the observed x-ray pulsations result from time-dependent scattering of the emission within the closed magnetosphere (Fig. 4B)—a scenario similar to that proposed to explain magnetospheric eclipses of pulsed radio emission in the double pulsar system PSR J0737–3039 (*28*, *29*). If so, then the observed thermal emission in the Q mode is only about half the actual hotspot emission, doubling the inferred area of the hotspot.

If scattering plays an important role in the Q mode, the absence of x-ray pulsations and thermal x-rays in the B mode may be attributed to increased scattering. As suggested to explain nulling and mode switching in radio pulsars (*30*), an expansion in the volume of the closed magnetosphere might accompany the mode change, although it is unlikely to achieve the required degree of screening. It thus appears that at B-mode onset, the surface hotspot emission is reduced to undetectable levels within a few seconds, induced by a drastic reduction in the downward flow of charged particles.

In the context of the polar gap model, it has been suggested (*31*) that mode changes occur when the local surface temperature crosses a critical value, ~10^6 K, that separates dominant emission mechanisms. This would require hotspots to be detectable in both modes, in contradiction with our results. B-mode emission may represent a cooler mode where curvature radiation dominates. However, the temperature transition remains unexplained, and our results strongly suggest that a global rather than local mechanism is

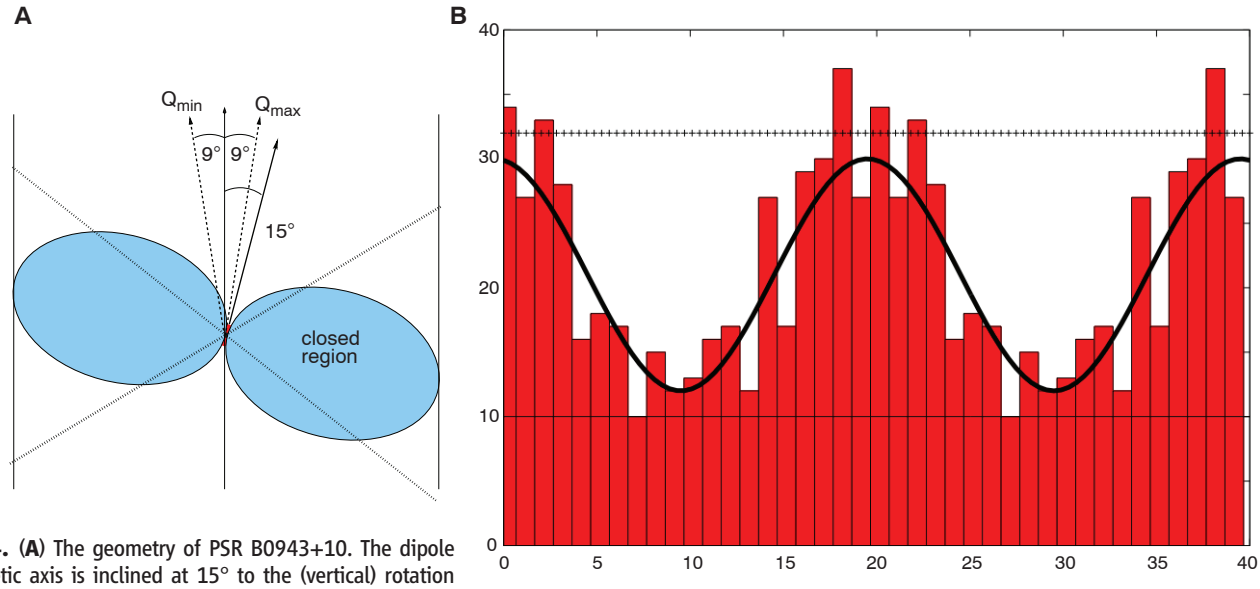

Fig. 4. (**A**) The geometry of PSR B0943+10. The dipole magnetic axis is inclined at 15° to the (vertical) rotation axis; the diagonal lines indicate the location of the null-charge surface, separating regions of positive and negative charge. As the pulsar rotates, the observer's line of sight maintains an angle of 9° to the rotation axis, with Q_{max} indicating the alignment when the radio pulse is seen (in both modes). The blue region indicates the supposed closed region, bounded by the light cylinder (at which the corotating magnetosphere reaches a rotation velocity equal to the speed of light) at 52,000 km. (**B**) If, in a toy model, extinction of thermal x-rays from the polar cap is proportional to the extent of the traversed closed region (~10,000 km at Q_{min} and ~500 km at Q_{max}), then we obtain a sinusoidal fit to the observed Q-mode x-ray pulse, so that maximum recorded emission corresponds to minimum extinction and vice versa. The lower horizontal line corresponds to the level of steady nonthermal emission and demonstrates that extinction of the thermal emission is near total at Q_{min}. The upper horizontal line then represents the level of actual unscattered x-ray emission from the polar cap.

required. Indeed, for a near-aligned pulsar such as PSR B0943+10, a range of quasi-stable magnetospheric configurations is expected (*32*, *33*), and the nonlinear system is proposed to suddenly switch between specific states, each having a specific emission beam and spin-down rate (*30*).

Whatever the true nature of the mode switch, the contrast between the Q mode's enhanced x-ray emission and reduced radio emission may well be illusory. Radio emission is only sampled on field lines instantaneously directed toward us, and our line of sight (*34*) makes only a grazing traverse of the polar cap. The core region of this polar cap, the probable site of x-ray hotspots, remains invisible to us at radio frequencies and may well change differently.

The totality of the mode transition in PSR B0943+10—changes in radio subpulse behavior and profile, the appearance of a precursor and, now, the switching on and off in x-rays of a likely hotspot—implies that we are dealing with a rapid and global magnetospheric state change. Through radio and x-ray "before" and "after" snapshots, we have shown that a magnetosphere 10 times the size of Earth completely changes personality within a few seconds; such a near-instantaneous transformation challenges our current understanding of pulsars and magnetospheres in general.

References and Notes

1. M. Ruderman, P. Sutherland, *Astrophys. J.* **196**, 51 (1975).
2. J. Arons, E. T. Scharlemann, *Astrophys. J.* **231**, 854 (1979).
3. D. C. Backer, *Nature* **228**, 42 (1970).
4. K. H. Hesse, R. Wielebinski, *Astron. Astrophys.* **31**, 409 (1974).
5. M. Kramer, A. G. Lyne, J. T. O'Brien, C. A. Jordan, D. R. Lorimer, *Science* **312**, 549 (2006).
6. F. Camilo, S. M. Ransom, S. Chatterjee, S. Johnston, P. Demorest, *Astrophys. J.* **746**, 63 (2012).
7. D. R. Lorimer *et al.*, *Astrophys. J.* **758**, 141 (2012).
8. A. Lyne, G. Hobbs, M. Kramer, I. Stairs, B. W. Stappers, *Science* **329**, 408 (2010).
9. A. A. Abdo *et al.*, *Astrophys. J. Suppl. Ser.* **187**, 460 (2010).
10. A. Shearer *et al.*, *Science* **301**, 493 (2003).
11. S. A. Suleymanova, V. A. Izvekova, *Sov. Astron.* **28**, 32 (1984).
12. J. M. Rankin, S. A. Suleymanova, *Astron. Astrophys.* **453**, 679 (2006).
13. I. Backus, D. Mitra, J. Rankin, *Mon. Not. R. Astron. Soc.* **404**, 30 (2010).
14. B. Zhang, D. Sanwal, G. G. Pavlov, *Astrophys. J.* **624**, L109 (2005).
15. J. Gil, G. Melikidze, B. Zhang, *Astrophys. J.* **650**, 1048 (2006).
16. See supplementary materials on *Science* Online.
17. G. Hobbs, A. G. Lyne, M. Kramer, C. E. Martin, C. Jordan, *Mon. Not. R. Astron. Soc.* **353**, 1311 (2004).
18. L. Strüder *et al.*, *Astron. Astrophys.* **365**, L18 (2001).
19. M. J. L. Turner *et al.*, *Astron. Astrophys.* **365**, L27 (2001).
20. W. Becker *et al.*, *Astrophys. J.* **615**, 908 (2004).
21. J. Gil *et al.*, *Astrophys. J.* **686**, 497 (2008).
22. W. W. Zhu *et al.*, *Astrophys. J.* **734**, 44 (2011).
23. J. Gil, M. Sendyk, *Astrophys. J.* **541**, 351 (2000).
24. A. A. Deshpande, J. M. Rankin, *Mon. Not. R. Astron. Soc.* **322**, 438 (2001).
25. A. K. Harding, A. G. Muslimov, *Astrophys. J.* **568**, 862 (2002).
26. B. Zhang, A. K. Harding, *Astrophys. J.* **532**, 1150 (2000).
27. J. M. Rankin, *Astrophys. J.* **405**, 285 (1993).
28. M. Lyutikov, C. Thompson, *Astrophys. J.* **634**, 1223 (2005).
29. R. P. Breton *et al.*, *Astrophys. J.* **747**, 89 (2012).
30. A. N. Timokhin, *Mon. Not. R. Astron. Soc.* **408**, L41 (2010).
31. B. Zhang, G. J. Qiao, W. P. Lin, J. L. Han, *Astrophys. J.* **478**, 313 (1997).
32. S. P. Goodwin, J. Mestel, L. Mestel, G. A. E. Wright, *Mon. Not. R. Astron. Soc.* **349**, 213 (2004).
33. A. N. Timokhin, *Mon. Not. R. Astron. Soc.* **368**, 1055 (2006).
34. J. M. Rankin, *Astrophys. J.* **301**, 901 (1986).

Acknowledgments: We thank the staff of XMM-Newton, GMRT, and LOFAR for making these observations possible. XMM-Newton is an ESA science mission with instruments and contributions directly funded by ESA member states and by NASA. GMRT is run by the National Centre for Radio Astrophysics of the Tata Institute of Fundamental Research. LOFAR, the Low Frequency Array designed and constructed by ASTRON, has facilities in several countries that are owned by various parties (each with their own funding sources) and are collectively operated by the International LOFAR Telescope (ILT) foundation under a joint scientific policy. ASTRON and SRON are supported financially by the Netherlands Organization for Scientific Research (NWO). Two of us (J.M.R., G.A.E.W.) thank NWO and ASTRON for visitor grants. C.F. was supported by Agence Nationale de la Recherche grant ANR-09-JCJC-0001-01. The used x-ray data can be retrieved from the XMM-Newton Science Archive at xmm.esac.esa.int/xsa. The applied B- and Q-mode window selections, derived from the GMRT and LOFAR observations, are listed in table S2.

Supplementary Materials

www.sciencemag.org/cgi/content/full/339/6118/436/DC1
Materials and Methods
Figs. S1 and S2
Tables S1 to S5
References (*35*–*40*)

1 October 2012; accepted 29 November 2012
10.1126/science.1230960